Dynamics and structural features of the microtubule plus-ends in interphase mouse fibroblasts
Zovko, S.

CHAPTER IV

Cryo-electron tomography of vitrified fibroblasts: microtubule plus ends *in situ*

Roman I. Koning, Sandra Zovko, Montserrat Bárcena, Gert T. Oostergetel, Henk K. Koerten, Niels Galjart, Abraham J. Koster and A. Mieke Mommaas

Cryo-electron tomography of vitrified fibroblasts: microtubule plus ends *in situ*

M*ouse Embryonic Fibroblasts (MEFs) are cells that have highly suitable biophysical properties for cellular cryo-electron tomography. MEFs can be grown directly on carbon supported by EM grids. They stretch out and grow thinner than 500 nm over major parts of the cell, attaining a minimal thickness of 50 nm at their cortex. This facilitates direct cryo-fixation by plunge-freezing and high resolution cryo-electron tomography. Both by direct cryo-EM projection imaging and cryo-electron tomography of vitrified MEFs we visualized a variety of cellular structures like ribosomes, vesicles, mitochondria, rough endoplasmatic reticulum, actin filaments, intermediate filaments and microtubules.*

MEFs are primary cells that closely resemble native tissue and are highly motile. Therefore they are attractive for studying cytoskeletal elements. Here we report on structural investigations of microtubule plus ends. We were able to visualize single frayed protofilaments at the microtubule plus end in vitrified fibroblasts using cryo-electron tomography. Furthermore it appeared that MEFs contain densities inside their microtubules, although 2.5 to 3.5 times less than in neuronal cells (Garvalov et al., 2006). Projection imaging of cellular microtubule plus ends showed that 40% was frayed, which is two times more than expected when compared to microtubule growth and shrinkage rates in MEFs. This suggests that frayed ends might be stabilized in the cell cortex.

Introduction

Electron tomography of cells is unique in enabling three-dimensional imaging of structures and their interactions inside the cell at nanoscale resolution. Cryofixation of cells bypasses chemical fixation and enables preservation of fast cellular processes. In addition, it is not required to add stain to outline structures of interest for imaging of cryofixed material with cryo-electron microscopy. This prevents resolution limitations and complications in interpretation of stain distribution, enabling to study of molecular structures and molecular interactions. Combined with cryo-electron tomography this ensures the best imaging possibilities of cellular structures (Koster A.J. and Barcena M, 2007; Plitzko and Baumeister, 2006). Following this approach, it is in principle possible to localize macromolecular complexes in the tomograms. By matching these complexes with higher resolution models obtained with e.g. crystallography or single particle electron microscopy these structures can be identified in the tomograms (Frangakis et al., 2002; Ortiz et al., 2006; Seybert et al., 2006). This can help enormously to improve our understanding of their function *in situ*.

Apart from the above mentioned advantages of cryo-electron tomography, several drawbacks of the approach may limit the applicability of the method. The thickness of samples imposes severe constraints in electron tomography. First, electrons have a limited mean free path when traversing through the specimen. The effective thickness increases drastically at the high tilt angles needed for tomography, becoming twice the original thickness at 60° and almost three times at 70°. This restricts the usable object thickness to about a few hundred nanometers, depending on the high-voltage of the electron microscope and the type of specimen (Grimm et al., 1996; Koster et al., 1997). Second, the resolution attainable in tomography is intrinsically dependent on the thickness of the sample (Crowther et al., 1970). Consequently, the attainable resolution is higher in thinner samples –given the same number of initial images and the same collection scheme. This factor becomes especially critical in cryo-electron tomography, where the limited dose that can be applied also poses a restriction to the number of images.

Because of the thickness restriction, the amount of different cell types that can be vitrified and imaged as a whole with electron tomography is very limited. As a result, the number of published studies where whole cell tomography plays an important role is restricted to small prokaryotic cells (usually archaebacteria) (Grimm et al., 1998; Murphy et al., 2006; Ortiz et al., 2006; Seybert et al., 2006). For the vast majority of eukaryotic cells, most areas other than the cortex are usually too thick for direct imaging. To overcome the thickness restriction the alternatives are to either restrict tomography to structures that are present near the plasma membrane (Medalia et al., 2002; Medalia et al., 2007) or to cryo-section the material (Al Amoudi et al., 2005; Dubochet et al., 1988; Hsieh et al., 2006). The latter approach has increasingly improved over the years and still holds an enormous potential, yet is not exempt of compression and cutting artifacts, and remains technically quite challenging. In this regard, a biological system that allows access to a large area of plunge-frozen eukaryotic cells without the need of sectioning would be advantageous. Here we report on our experience on exploring the advantages of primary mouse embryonic fibroblasts (MEFs) for cryo-electron tomography.

MEFs are primary cells and closely resemble the native tissue that they are derived from. They can easily grow on substrates that are used for light (coated or uncoated

glass) and electron microscopy (carbon). MEFs are motile cells which makes them an attractive model for studying cell motility and microtubules (Akhmanova et al., 2001; Akhmanova and Hoogenraad, 2005; Vidali et al., 2006). MEFs have the special feature that they grow flat in vast regions. Therefore the microtubule network is easily detectable by both LM and EM. This makes it possible to study individual microtubules, which for example is difficult in the narrow dendritic and axonal parts of neurons.

Microtubules are highly dynamic structures that continuously change between growing and shrinking stages. These stages can be discerned using cryo-electron microscopy since each microtubule state shows a specific structure at their plus-end. *In-vitro* studies (Mandelkow et al., 1991; O'toole et al., 2003b) showed that shrinking ends are frayed and growing ends have a sheetlike appearance. In several microtubule studies (Hoog et al., 2007; O'toole et al., 2003b; Austin et al., 2005; Vandenbeldt et al., 2006) it was suggested that the *in-vitro* relation between microtubule plus end structure and dynamics is not necessarily identical to the situation *in-vivo,* where microtubule dynamics is regulated by a variety of microtubule associated proteins.

We investigated the microtubule plus end structures in the thinnest parts of MEFs. Here not only typical cortical cellular structures like microtubules and actin were observed, but also mitochondria, rough endoplasmatic reticulum and several vesicular structures. Microtubule plus ends were directly visible in untilted cryo-electron microscopy images of vitrified cells that were grown on electron microscopy grids. From these images the amount of shrinking microtubules were quantified. Additionally high resolution cryo-electron tomograms were collected showing single curved protofilaments at the microtubule plus end *in situ*. Also it was shown that MEFs contain densities inside the microtubules, like was demonstrated recently for neuronal cells (Garvalov et al., 2006). Furthermore, cryo-electron tomography of relatively large structures like mitochondria inside whole vitrified cells could be performed.

Materials and Methods

Cell culture

Mouse embryonic fibroblasts (MEFs) were cultured in a 1:1 mixture of Dulbecco's modified Eagle's medium (DMEM) (GIBCO, Invitrogen, The Netherlands) and Ham's F10 medium (Cambrex, U.S.A.), supplemented with 10% fetal calf serum and antibiotics, in a humidified atmosphere with 5% CO_2 at 37°C. MEFs were grown on Thermanox coverslips (NUNC, Naperville, U.S.A.) for two days. For cryo-electron microscopy and tomography MEFs were grown overnight on carbon coated formvar that was supported by a gold EM grid.

Sample preparation for transmission electron microscopy

For cryo-electron tomography, 10 nm colloidal gold particles were used as fiducial markers. They were added to the formvar side of the grid before cell growth. Excess medium was automatically blotted off in an environmentally controlled chamber operated at 37°C and 100% humidity. Subsequently, the cells were cryo-fixed by plunging into liquid ethane. Samples were stored in liquid nitrogen.

Cells were cryo-fixed on the coverslips by plunge-freezing. Samples were freeze-substituted in 0.01% OsO_4 and 0.25% uranyl acetate in absolute acetone using an automatic freeze substitution apparatus (EM AFS, Leica Microsystems, Wetzlar, Germany) for three days at -90°C. The temperature was gradually raised to -20°C and subsequently maintained at -20°C for 12 hours. Finally the temperature was raised to 0°C with a rate of 10 degrees per hour. The cells were then washed twice for 15 minutes with acetone, infiltrated with epoxy resin at the RT and flat embedded. Thin sections (100 nm) were post-stained with uranyl acetate and a mixture of lead salts.

Sample preparation for scanning electron microscopy

Cells were then washed with PBS and fixed with 1.5% glutaraldehyde in 0.1 M cacodylate buffer (pH 7.2) for one hour at RT. This was followed by a wash step with PBS and a dehydration series by incubating the cells in 50%, 70%, 80%, 90% ethanol (each step 5 minutes) followed by incubation with 100% ethanol for 30 minutes, twice. The cells were then critical point dried in 100% ethanol using a Bal-Tec CPD030. Subsequently, specimens were coated with a layer of gold/palladium.

Sample preparation for fluorescence microscopy

To visualize the microtubule network in MEFs, immunofluorescence microscopy was performed. For this purpose, MEFs were grown overnight on glass coverslips. Cells were then washed in PBS at RT and fixed with cold methanol at -20°C. After washing in PBS, cells were incubated in blocking buffer for 45 minutes at RT. The cells were incubated with primary antibodies against tyr- tubulin (rat monoclonal, clone YL1/2, Abcam, Cambridge, U.K.), diluted 1:500 in blocking buffer, and against EB1 (mouse monoclonal, Transduction laboratories) diluted 1:150 in blocking buffer, for one hour at RT. The samples were washed three times for 15 minutes in PBS/0.05% Tween-20 and then incubated with goat-anti-rat-Alexa Fluor 488 and goat-anti-mouse-Alexa594 (both Molecular Probes) secondary antibody (1:200) for one hour at RT. Next, cells were washed three times in PBS/0.05% Tween-20, and in 70% and 100% ethanol, air dried and mounted onto the glass slide using Vectashield mounting medium with DAPI nuclear staining (Vector Laboratories, U.K.).

Electron microscopy

Cryo-electron tomography of cytoskeletal elements and mitochondria (Figure 3) was performed on a FEI Tecnai F20 microscope at 200 keV (FEI Company, Eindhoven, The Netherlands), equipped with a 1k x 1k Gatan CCD camera type 794 (Gatan, Pleasanton, USA). Tilt series were taken using Explore 3D software (FEI), at a defocus of -8 micron, every 3° from -54° to +54° at 14.500x magnification, resulting in a pixel size of 1.3 nm at the specimen level.

Cryo-electron tomography of microtubules in vitrified MEFs (Figure 4) was performed on a FEI Polara F30 microscope at 300 keV, equipped with a 2k x 2k Gatan camera with energy filter. Tilt series were taken using Explore 3D software, at a defocus of -4 micron, every 2° from -70° to +70° using a total dose of about 100 e/A^2 at 50.000x magnification. The pixel size was 0.6 nm at the specimen level.

For direct visualization of microtubule plus ends inside MEFs adjacent images were taken, forming a continuous area of several hundred square microns. Images were taken

on a 2k x 2k camera with a GATAN 2002 image filter at 14.000x on a FEI Tecnai F20 microscope at 200 keV.

The thin sections of flat embedded MEFs were analyzed on a Philips CM10 Transmission Electron Microscope with a LaB_6 filament operating at 80kV. SEM was performed on a JEOL 6700F at 5kV.

Fluorescence microscopy

Immunofluorescent images were taken using a Leica DMRXA microscope with a Coolsnap K4 camera using ColorPro software.

Image analysis and visualization

Tomographic tilt series were processed using IMOD versions 3.5 to 3.9 (Kremer et al., 1996). Projection images were preprocessed by hot pixel removal and rough alignment by cross-correlation. Final alignment was done using the fiducial gold markers. The tomograms were obtained using weighted back-projection. Cryo-electron tomograms were Fourier filtered and denoised with a non-linear anisotropic diffusion (Frangakis and Hegerl, 2001) to enhance the visibility of structures. For 3D surface rendering the tomographic volumes were imported into AMIRA (Mercury Computer Systems, Merignac, France) for further processing and representation.

Microtubule plus end structures were categorized into three main categories: frayed, blunt and sheets. Microtubules with at least one frayed side were classified as frayed ends and are thought to represent shrinking microtubules. Microtubules of which one side was at least 25 nm longer than the other side and had no frayed ends were classified sheets. Microtubules that had two straight sides that were within 25 nm of each other and had no frayed ends were classified as blunt.

Results and Discussion

Mouse embryonic fibroblasts grow thin over large areas

A disadvantage of mammalian cells in their use for cryo-electron tomography is that they are usually too thick for direct imaging. When primary MEFs are grown on carbon supported by gold grids and on thermanox coverslips they spread and their diameter increased to several tens to hundreds of microns (Figure 1f-h). Moreover, MEFs appeared to grow thin over large cell areas. Cytoskeletal bundles were observed directly through the membrane at the cell cortex using SEM (Figure 1g-h). To accurately determine the cell thickness over larger areas, MEFs were grown on thermanox, flat embedded and cut perpendicularly (Fig. 1a). It appeared that the thickness of MEFs gradually decreased from
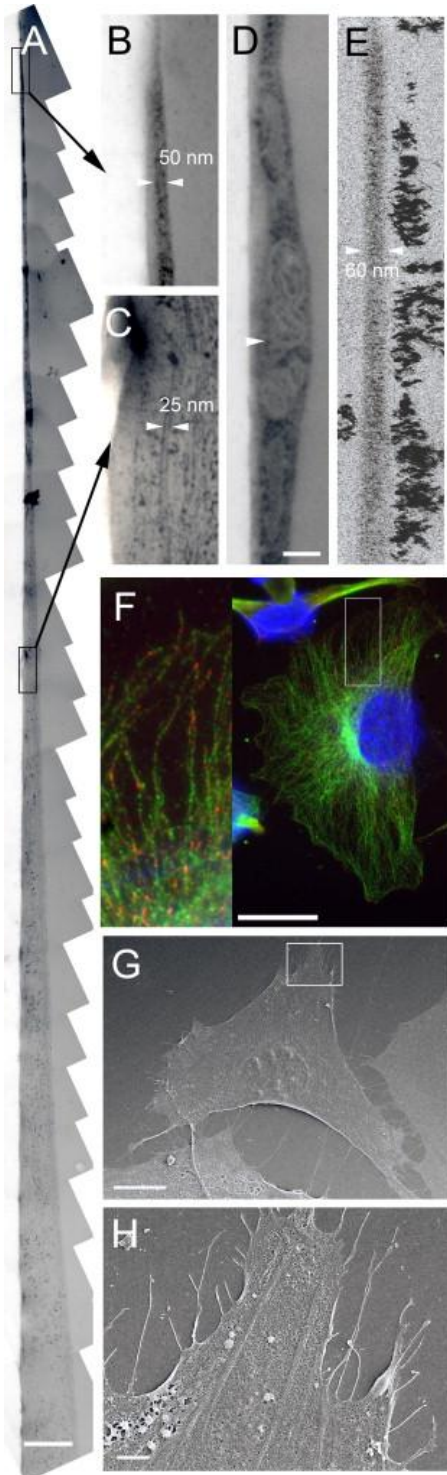
Figure 1. The thickness of mouse embryonic fibroblasts measured and visualized by several microscopy methods. a) Perpendicular cross section of a flat embedded MEF shows that cells can grow flat in extended regions of the cell and become exceedingly thin at the cell cortex. Scale bar is 1 micron. b) The cortex (enlarged from top black box in Figure a) shows that MEFs can become as thin as 50 nm directly at the cell boundary. c) Microtubules are present in parts of the cell that are less than 200 nm in thickness (enlarged bottom black box from Figure a). d) Perpendicular cross section of flat embedded MEF shows that the cell membrane can fold around large structures like mitochondria (white arrowhead). Scale bar is 1 micron. e) Digital density average along the YZ plane of a cryo-electron tomographic reconstruction shows that MEFs can grow as thin as 60 nm. Black densities are ice contaminations that were specific for this dataset. f) Fluorescence light microscopy image of MEFs. Microtubules are depicted in green, EB1 (End-Binding protein 1, a microtubule plus end binding protein) in red and the nucleus in blue. Individual microtubules can be discerned in the cell. Scale bar is 50 □m. The inset on the left is 4x magnified. g) SEM image of a MEF grown on thermanox shows that the cell, including the nucleus is extensively flattened. Scale bar is 20 micron. h) At the cell cortex (enlargement of white box in g) cytoskeletal bundles are clearly visible through protrusions of the cellular membrane. Scale bar is 2 □m.

several microns at the cell nucleus to a minimal height of 50 nm at their boundary. This minimal thickness corresponded well to measurements that were determined on cryo-electron tomograms of vitrified cells that were grown on grid (Fig. 1e). Here the thinnest measured area was 60 nm, which can accommodate no more than two microtubules. Since the thickness of MEFs increased gradually towards the nucleus, large areas of the cells measured less than several hundred nanometers in thickness. Occasionally cellular components like vesicles or mitochondria protruded the cell membrane, making the cell locally thicker than its surroundings (Fig. 1d). The limited thickness of MEFs is an important advantage for cryo-electron microscopy studies, allowing vitrification by straightforward plunge freezing after directly growing them on EM grids. Also, individual microtubules can be visualized separately in the cell cortex when visualized by fluorescence light microscopy (Fig 1e) (Peris et al., 2006). This is useful for microtubule localization by fluorescence microscopy and in correlation of fluorescence and electron microscopy images.

Cellular content of vitrified MEFs can be directly observed by cryo-EM
The limited thickness of the MEFs has two other advantages. First, it enables direct observation of cellular contents in cryo-electron microscopy projection images (Fig. 2). The structures that are observed in the thinnest cell areas near the cell plasma membrane are mainly ribosomes, actin and small lipid vesicles (Fig. 2a). Further away from the cell boundary, larger cellular structures like mitochondria, rough endoplasmatic reticulum and microtubules can directly be visualized in their native environment (Fig. 2b). Surprisingly, in these areas the protofilaments that comprise the microtubules are easily discerned (Fig. 2c). The limited thickness of the cells allows high resolution 3D imaging since the object thickness is directly related to the maximum resolution that can be attained (Crowther et al., 1970). Therefore in the thinner parts of MEFs high resolution information can be attained *in situ* of thin cytoskeletal structures, like microtubules. Second, up to now cellular cryo-electron tomography was mainly restricted to small cells like archaebacteria (Comolli et al., 2006; Hoog et al., 2007; Nicastro et al., 2000; Nickell et al., 2003; Seybert et al., 2006). These MEFs also permit primary mammalian cells to be used in cryo-electron tomography in cellular regions other than commonly used protruding filopodia or dendrites. Therefore also a wider variety of cellular structures can be imaged *in situ*.

Cryo ET reconstructions of cytoskeletal elements and mitochondria
Figure 3 shows some examples of cryo-electron tomographic reconstructions of actin (Fig. 3a and c), intermediate filaments (Fig. 3b), microtubules (Fig. 3c) and mitochondria (Fig. 3d) in vitrified cells that were grown on carbon supported by EM grids. The structural organization of cytoskeletal components is clearly visible, while additionally ribosomal subunits can be visualized. A tomographic slice of cellular actin in protrusions shows branching of actin filaments (Fig. 3a and c) as was observed earlier in *Dictyostelium* cells (Medalia et al., 2002). Actin filaments seem to induce outward indentation of the membrane and densities are present on the outside of the filopodia membrane (Fig. 3a). Cryo-electron tomographic slices show frayed protofilaments at the plus ends and densities that are present inside the microtubules (Fig. 3c and Fig. 5).

Also relatively large cellular structures like rough endoplasmatic reticulum (data not shown) and mitochondria were reconstructed *in situ* by cryo-electron tomography (Fig. 3d). Tomograms of
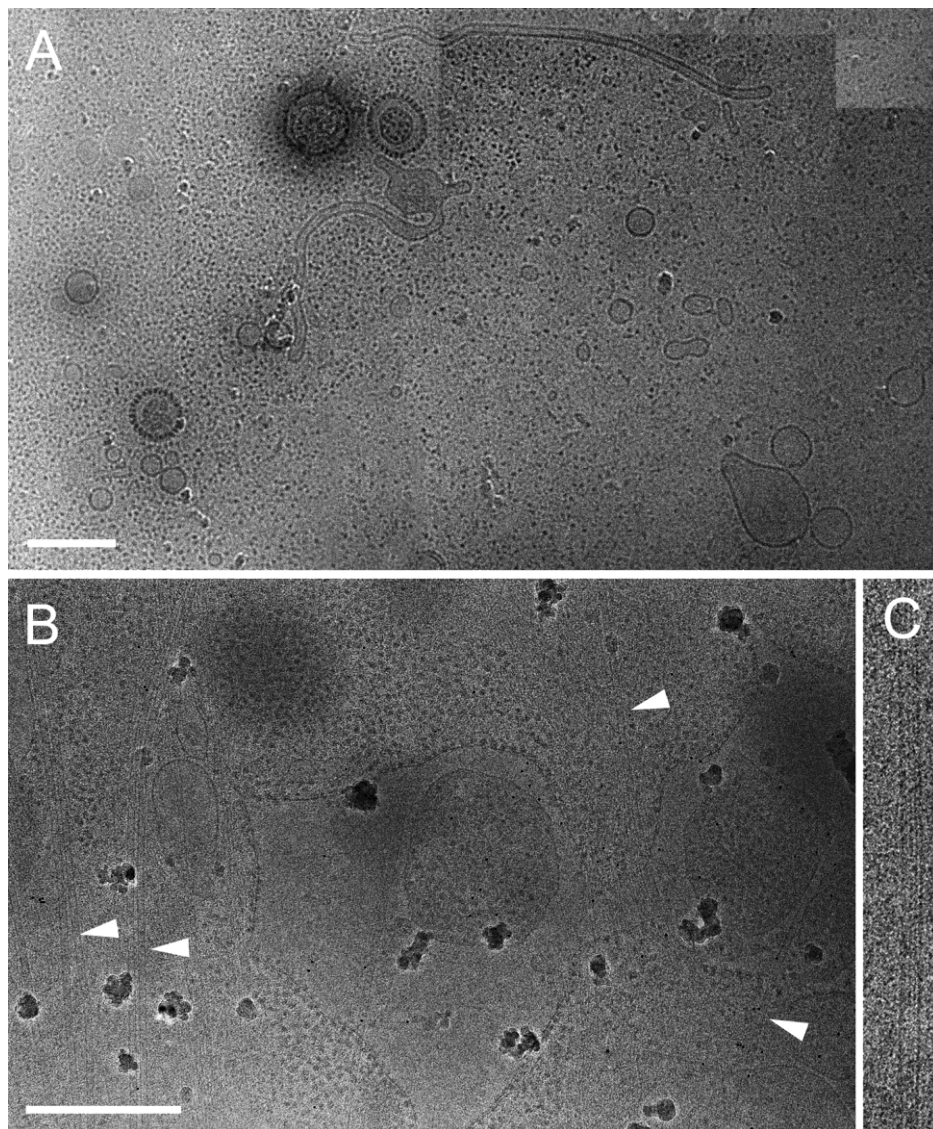
Figure 2. Cryo-electron microscopy images of thin areas in the cortex of mouse embryonic fibroblasts that were grown on formvar supported carbon on an EM grid. a) Montage of CCD images show that at the cortex ribosomes (small dark spots), endosomes like structures, coated vesicles and fusing or pinching vesicles (bottom right) can be directly observed. Scale bar is 500 nm. b) Further away from the cell border larger structures like rough endoplasmatic reticulum and microtubules (white arrows) can be observed. Scale bar is 500 nm. c) Microtubule protofilaments can be observed directly inside vitrified cells.

mitochondria showed cristae and sometimes high density inclusions (Fig. 3d) that were also observed in plastic embedded sections of similar cells.
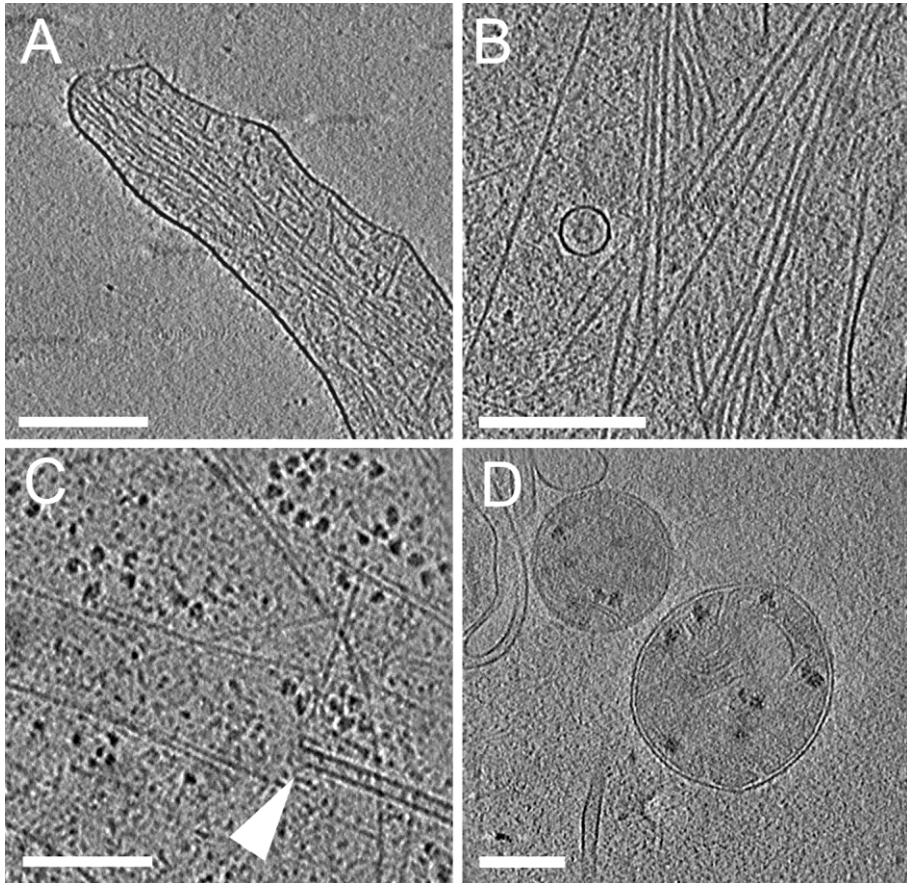
Figure 3. Cryo-electron tomographic slices of cellular organelles and cytoskeletal structures in mouse embryonic fibroblasts. a) Actin filaments in a cell protrusion. b) Intermediate filaments. c) Microtubule plus end (white arrow), actin and ribosomes. d) Mitochondria. The digital sections through the tomogram are respectively 13nm, 16.5 nm, 10.6 nm and 16.5 nm thick. All scale bars are 200 nm.

Microtubule plus end structure in situ

Microtubule plus ends were localized in vitrified MEFs by direct imaging in low dose search mode using an energy filter at a magnification of around 9000x (Fig. 4a). At lower magnifications it was difficult to locate microtubules with certainty. Using cryo-electron tomography of vitrified MEFs we were able to visualize microtubule plus ends at the level of the protofilaments *in situ* (Fig 4. d-g). Two individual protofilaments at the microtubule plus end that were curving outwards from the microtubule were discerned in orthogonal directions. Both in z- and y-slices the frayed protofilaments were clearly visible (Fig. 4d-e). By projecting a 120 nm long stretch in the axial direction of the microtubule the 13

protofilaments that make up the microtubule (Fig. 4c). From the first image in figure 4D, where the individual protofilaments can be observed we estimate that the resolution perpendicular to the tilt axis is around 5 nm (the protofilament spacing). The resolution along the z-slices is clearly less than 5 nm, since in that direction the individual protofilament inside the microtubule lattice could not be distinguished (Fig 4c). Nevertheless, we were still able to visualize the curved protofilament at the microtubule plus end in the z-direction (Fig. 4e), since it was not surrounded by other density. A hand-drawn surface representation of the microtubule also shows the orthogonal positioning of the protofilaments (Fig. 4 f and g). In embedded and stained sections, microtubule plus ends were visualized earlier embedded in the kinetochore (O'toole et al., 2003a; Austin et al., 2005; Vandenbeldt et al., 2006). Recent cryo-electron tomographic reconstructions of microtubules (Bouchet-Marquis et al., 2007; Nicastro et al., 2006; Sui and Downing, 2006) were able to discern the individual protofilaments of microtubules but did not show protofilaments at the plus end.

The visualization of individual protofilaments inside vitrified MEFs is a first step towards the investigation of different microtubule plus end conformations *in situ*. The frayed protofilaments we observed at the microtubule plus ends were shown to be indicative for shrinking microtubules by *in-vitro* studies (Mandelkow et al., 1991). However the link between the structure of the protofilaments at the microtubule plus end and its dynamics as determined *in-vitro* is not necessarily identical *in-vivo*. Plus end structures might be influenced by the stabilizing or destabilizing properties of proteins that are present in the cell. Hoog et al. recently suggested that in *S.pombe* flared ends might represent growing microtubules (Hoog et al., 2007). Also it has been suggested that frayed microtubules actually are stabilized in the kinetochore (Vandenbeldt et al., 2006).

Densities inside microtubules

In all microtubules that were present in our tomograms of MEFs we observed luminal densities in the interior of microtubules (Fig. 3c, 4d-h). Because of the small mass of these densities, they only appeared in tomographic slices and were not visible in two-dimensional cryo-electron microscopy projections. Densities inside microtubules were reported earlier and visualized recently (Garvalov et al., 2006; Bouchet-Marquis et al., 2007) in rat embryonic hippocampal neurons. Garvalov et al. were not able to confirm the presence of similar densities inside epithelial cell lines, such at PtK2 and HeLa cells. This

might be due to the limited resolution caused by the thickness of the cells or a smaller size of the luminal particles.

We show here that densities inside microtubules are also present in primary cultured mouse embryonic fibroblasts. The luminal microtubule densities in MEFs appear smaller (~ 4-6 nm) than in hippocampal neurons (~ 6-7 nm). On average microtubules from MEFs contained 21.0 particles per micrometer while their mean distance was 47.6 nm (160 particles were counted in microtubules with a total length of 7.612 micron). The abundance of luminal particle in MEF microtubules was clearly less than in neuronal cells (68.3 to 111.0 particles per micrometer) and in P19 stem cells (51.8 particles per micrometer; Table 1 in Garvalov et al). Furthermore in microtubules from MEFs they did
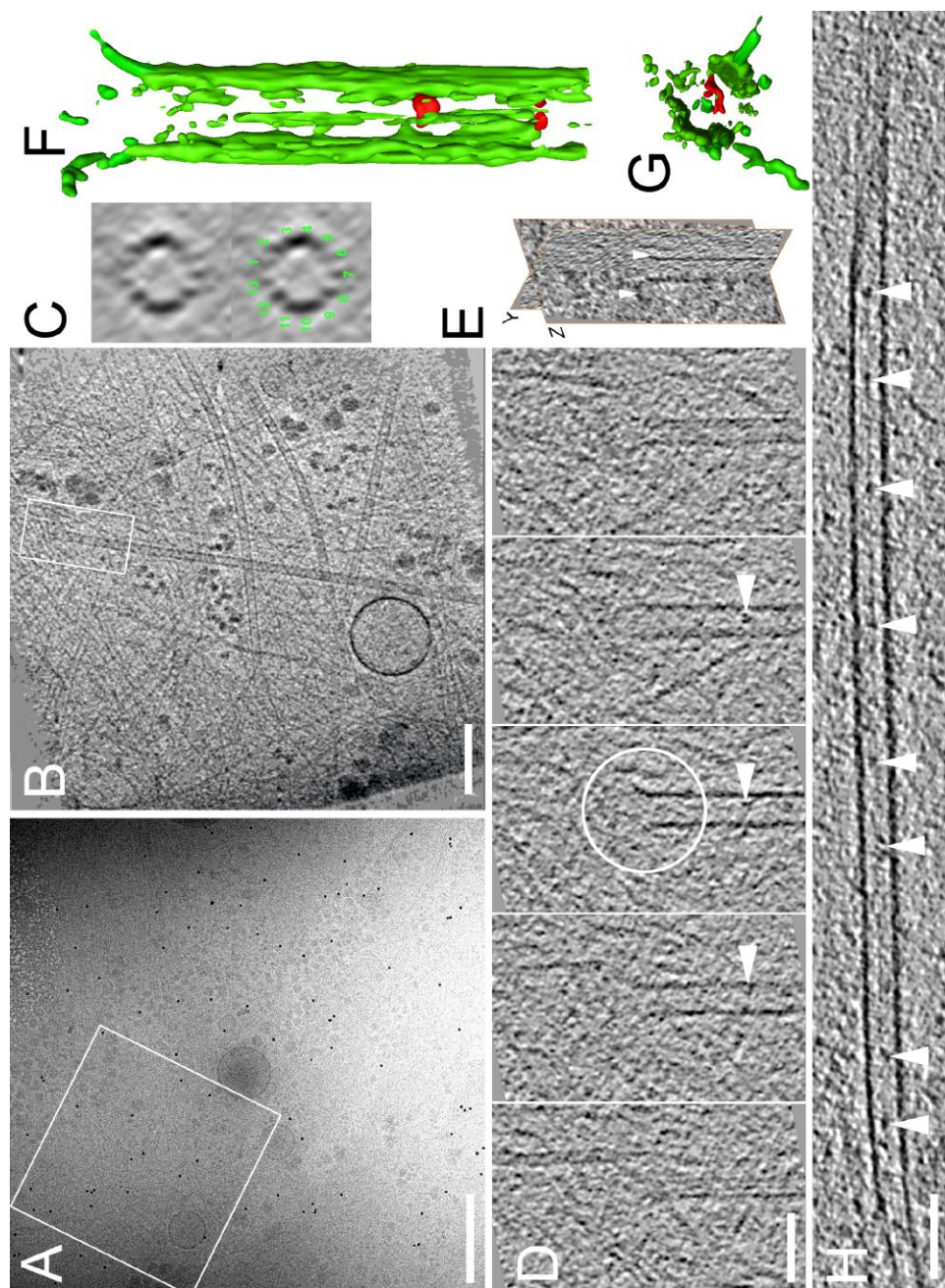
Figure 4. Cryo-electron tomography of microtubules inside MEFs. a) Low magnification overview recorded at 9000x magnification in search mode of low dose to localize microtubules. Scale bar is 500 nm. b) Tomographic z-slice constituting the whole cell thickness (~90 nm). The white box in a) denotes the position where the tomogram was taken. Scale bar is 200 nm. c) Tomographic slice

along the microtubule direction of 120 nm thickness. The 13 protofilaments are indicated. d) Consecutive tomographic 5 nm thick z-slices from a microtubule plus end (white circle) *in situ* (enlarged from white box in b). The density of one or several overlapping curved protofilaments is visible in the middle slice. Individual protofilaments inside the microtubule can be observed in the first and last z-slices. The white arrowhead points to densities that were regularly observed inside microtubules. An intermediate filament (first slice) and an actin fiber that ends in close proximity to the microtubule (two last slices) can be observed next to the microtubule. e) Outward curving protofilaments (white arrowheads) can be observed in perpendicular slices along y and z directions. Scale bar is 50 nm. f) Drawn surface rendering interpretation shows frayed microtubule plus end and densities that are present inside microtubules (in red). g) Top view from f), clearly showing the protofilaments in perpendicular directions. h) Tomographic 5 nm z-slice from the middle of a microtubule containing densities inside the microtubule (white arrows). Scale bar is 50 nm.

not have an obvious equidistant spacing and they seemed to have different shapes, while in neurons they appeared similar in shape. Although it remains to be shown what the nature and function of these densities is, our results show that their presence is not restricted to neuronal cells alone. The existence of densities inside microtubules in different cell types indicates that they might be a general phenomenon. The observed differences in appearance, abundance and shape in fibroblasts compared to neurons, might indicate different functions in different cells.

Microtubule dynamics

To gain insight into microtubule dynamics we determined the shapes of the microtubule plus ends by direct cryo-EM observation of vitrified MEFs (Figure 5). In ~500 (mostly adjacent) images beholding ~1700 μm^2 of cell area we counted 106 microtubule ends. We observed 6 microtubules of which both ends were visible, so minimally 5.7% of the observed ends were microtubule minus ends that were not embedded in the centrosome.

In MEFs 40% of the microtubules had frayed ends, 35% had sheet-like ends and 26% was blunt.

Since the shrinkage rate of microtubules in MEFs is ~5/3 x higher than the growth rate (growth 21.5 ± 8.2 µm/min versus shrinkage: 35.6 ± 12.8 µm/min, (Komarova et al., 2002)) and the amount of microtubule ends in a cell is constant, less shrinking than growing microtubules are expected to be observed in a 3:5 ratio. Taking this into account, instead the amount of microtubules with frayed ends is two times higher than expected. This suggests that frayed microtubules can be stabilized by cellular structures as was suggested earlier for the kinetochore (Vandenbeldt et al., 2006).

Despite the limited cell thickness, individual protofilaments were not observed in projection images. More extensive cryo-electron tomography (as shown in Figure 4) should be performed to expand the structural information beyond the three major types of plus ends that were discriminated. In addition the proximity of specific microtubule plus ends structures (like e.g. frayed ends) to specific cellular structures (like e.g. actin or vesicles) can be investigated.
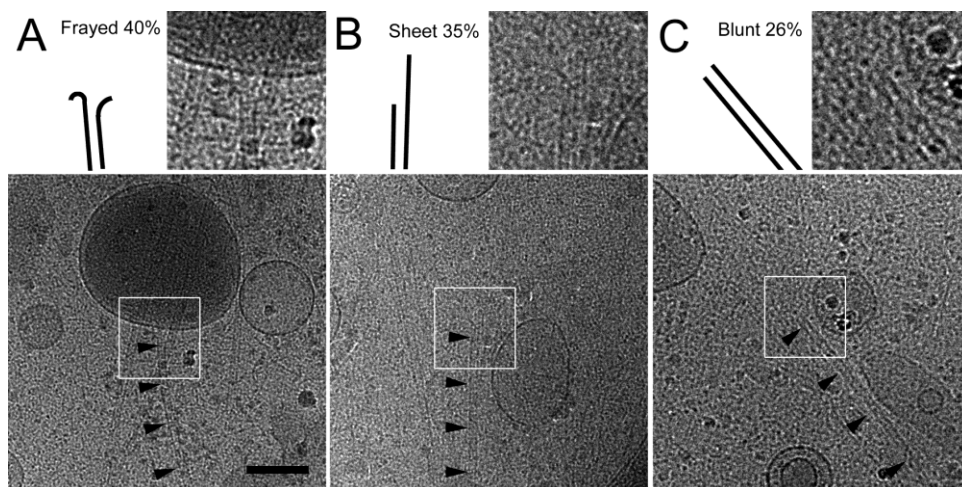
Figure 5. Cryo-electron microscopy images of microtubule plus end inside vitrified MEFs. a) Examples of a) a frayed end in the vicinity of a mitochondrion b) a sheet like microtubule end and c) a blunt end. Black arrowheads denote the microtubule. The white square encloses the area of the two times enlarged images on the top right. The schematic drawings of frayed, sheet and blunt microtubule ends represent the outline of the microtubule in the image on the top right. Scale bar is 200 nm.

Conclusion

We have grown primary mouse embryonic fibroblasts on carbon, supported by gold EM grids. The MEFs spread out and grew thin over vast areas, reaching a minimal thickness of 50 nm near the plasma membrane. The limited thickness enabled direct vitrification of the cells by plunge freezing. It also facilitated direct observation of cellular content by cryo-electron microscopy. Ribosomes, vesicular structures, rough endoplasmatic reticulum, mitochondria and all cytoskeletal components, including the protofilaments inside microtubules were visualized directly *in situ* in vitrified cells. Because of their thin character, MEFs are very suitable for cryo-electron tomography of microtubule plus ends. We were able to perform cryo-electron tomography of relatively large structures like mitochondria inside vitrified cells. Moreover, we could localize microtubule plus ends directly in vitrified cells and determined their structure using cryo-electron tomography. Hereby we visualized single protofilaments in orthogonal directions at the microtubule plus end *in situ*. Additionally, we showed that MEFs contain particles inside their microtubules, although to a lesser extent than neuronal cell types. Direct visualization of microtubule plus end conformations *in situ* allowed the investigation of microtubule dynamics. Almost half (40%) of the observed microtubule ends appeared to be shrinking while one third (35%) was growing. When compared to microtubule growth and shrinkage rates in MEFs this suggests that frayed ends might be stabilized by structures in the cell cortex.

References

Akhmanova,A., and C.C.Hoogenraad. 2005. Microtubule plus-end-tracking proteins: mechanisms and functions. Curr. Opin. Cell Biol. *17*:47-54.

Akhmanova,A., C.C.Hoogenraad, K.Drabek, T.Stepanova, B.Dortland, T.Verkerk, W.Vermeulen, B.M.Burgering, C.I.De Zeeuw, F.Grosveld, and N.Galjart. 2001. Clasps are CLIP-115 and -170 associating proteins involved in the regional regulation of microtubule dynamics in motile fibroblasts. Cell *104:*923-935.

Al Amoudi,A., L.P.O.Norlean, and J.Dubochet. 2005. Cryo-electron microscopy of vitreous sections of native biological cells and tissues (*vol 148*, pg 131, 2004). Journal of Structural Biology 149:225.

Austin,J.R., J.M.Segui-Simarro, and L.A.Staehelin. 2005. Quantitative analysis of changes in spatial distribution and plus-end geometry of microtubules involved in plant-cell cytokinesis. J. Cell Sci. *118*:3895-3903.

Bouchet-Marquis,C., B.Zuber, A.M.Glynn, M.Eltsov, M.Grabenbauer, K.N.Goldie, D.Thomas, A.S.Frangakis, J.Dubochet, and D.Chretien. 2007. Visualization of cell microtubules in their native state. Biol. Cell *99:*45-53.

Comolli,L.R., M.Kundmann, and K.H.Downing. 2006. Characterization of intact subcellular bodies in whole bacteria by cryo-electron tomography and spectroscopic imaging. J. Microsc. *223:*40-52.

Crowther,R.A., D.J.De Rosier, and A.Klug. 1970. The reconstruction of a three-dimensional structure from projections and its application to electron microscopy. Proc. Roy. Soc. Lond. *317*:319-340.

Dubochet,J., M.Adrian, J.J.Chang, J.C.Homo, J.Lepault, A.W.Mcdowall, and P.Schultz. 1988. Cryo-Electron Microscopy of Vitrified Specimens. Quarterly Reviews of Biophysics *21*:129-228.

Frangakis,A.S., J.Bohm, F.Forster, S.Nickell, D.Nicastro, D.Typke, R.Hegerl, and W.Baumeister. 2002. Identification of macromolecular complexes in cryoelectron tomograms of phantom cells. Proc Natl Acad Sci U S A *99:*14153-8.

Frangakis,A.S., andR.Hegerl. 2001. Noise reduction in electron tomographic reconstructions using nonlinear anisotropic diffusion. J. Struct. Biol. *135:*239-250.

Garvalov,B.K., B.Zuber, C.Bouchet-Marquis, M.Kudryashev, M.Gruska, M.Beck, A.Leis, F.Frischknecht, F.Bradke, W.Baumeister, J.Dubochet, and M.Cyrklaff. 2006. Luminal particles within cellular microtubules. J. Cell Biol. *174*:759-765.

Grimm,R., H.Singh, R.Rachel, D.Typke, W.Zillig, and W.Baumeister. 1998. Electron tomography of ice-embedded prokaryotic cells. Biophys J *74:*1031-42.

Grimm,R., D.Typke, M.Barmann, and W.Baumeister. 1996. Determination of the inelastic mean free path in ice by examination of tilted vesicles and automated most probable loss imaging. Ultramicroscopy *63*:169-79.

Hoog,J.L., C.Schwartz, A.T.Noon, E.T.O'toole, D.N.Mastronarde, J.R.McIntosh, and C.Antony. 2007. Organization of interphase microtubules in fission yeast analyzed by electron tomography. Dev. Cell *12:*349-361.

Hsieh,C.E., A.Leith, C.A.Mannella, J.Frank, and M.Marko. 2006. Towards high-resolution three-dimensional imaging of native mammalian tissue: electron tomography of frozen-hydrated rat liver sections. J. Struct. Biol. *153*:1-13.

Komarova,Y.A., A.S.Akhmanova, S.Kojima, N.Galjart, and G.G.Borisy. 2002. Cytoplasmic linker proteins promote microtubule rescue *in vivo*. J. Cell Biol. *159*:589-599.

Koster A.J., and Barcena M. 2007. Electron Tomography: Methods for three-dimensional visualization of structures in the cell. pp. 113-163. in: J.Frank (Ed.), Electron Tomography: Methods for Three-Dimensional Visualization of Structures in the Cell, Springer, NY, Springer, NY, pp. 113-163.

Koster,A.J., R.Grimm, D.Typke, R.Hegerl, A.Stoschek, J.Walz, and W.Baumeister. 1997. Perspectives of molecular and cellular electron tomography. J Struct Biol 120:276-308.

Kremer,J.R., D.N.Mastronarde, and J.R.McIntosh. 1996. Computer visualization of three-dimensional image data using IMOD. J. Struct. Biol. *116*:71-76.

Mandelkow,E.M., E.Mandelkow, and R.A.Milligan. 1991. Microtubule dynamics and microtubule caps: a time-resolved cryo-electron microscopy study. J. Cell Biol. *114*:977-991.

Medalia,O., M.Beck, M.Ecke, I.Weber, R.Neujahr, W.Baumeister, and G.Gerisch. 2007. Organization of actin networks in intact filopodia. Current Biology *17*:79-84.

Medalia,O., I.Weber, A.S.Frangakis, D.Nicastro, G.Gerisch, and W.Baumeister. 2002. Macromolecular architecture in eukaryotic cells visualized by cryoelectron tomography. Science *298*:1209-13.

Murphy,G.E., J.R.Leadbetter, and G.J.Jensen. 2006. *In situ* structure of the complete Treponema primitia flagellar motor. Nature *442*:1062-1064.

Nicastro,D., A.S.Frangakis, D.Typke, and W.Baumeister. 2000. Cryo-electron tomography of neurospora mitochondria. J. Struct. Biol. *129*:48-56.

Nicastro,D., C.Schwartz, J.Pierson, R.Gaudette, M.E.Porter, and J.R.McIntosh. 2006. The molecular architecture of axonemes revealed by cryoelectron tomography. Science *313*:944-948.

Nickell,S., R.Hegerl, W.Baumeister, and R.Rachel. 2003. Pyrodictium cannulae enter the periplasmic space but do not enter the cytoplasm, as revealed by cryo-electron tomography. J. Struct. Biol. *141*:34-42.

O'toole,E.T., K.L.McDonald, J.Mantler, J.R.McIntosh, A.A.Hyman, and T.Muller-Reichert. 2003a. Morphologically distinct microtubule ends in the mitotic centrosome of Caenorhabditis elegans. J. Cell Biol. *163*:451-456.

O'toole,E.T., K.L.McDonald, J.Mantler, J.R.McIntosh, A.A.Hyman, and T.Muller-Reichert. 2003b. Morphologically distinct microtubule ends in the mitotic centrosome of Caenorhabditis elegans. J. Cell Biol. *163*:451-456.

Ortiz,J.O., F.Forster, J.Kurner, A.A.Linaroudis, and W.Baumeister. 2006. Mapping 70S ribosomes in intact cells by cryoelectron tomography and pattern recognition. Journal of Structural Biology *156*:334-341.

Peris,L., M.Thery, J.Faure, Y.Saoudi, L.Lafanechere, J.K.Chilton, P.Gordon-Weeks, N.Galjart, M.Bornens, L.Wordeman, J.Wehland, A.Andrieux, and D.Job. 2006. Tubulin tyrosination is a major factor affecting the recruitment of CAP-Gly proteins at microtubule plus ends. J. Cell Biol. *174*:839-849.

Plitzko,J., and W.Baumeister. 2006. Cryoelectron Tomography. pp. 529-598. in: P.W.Hawkes, J.C.H.Spence (Eds.), Science of Microscopy, Springer, NY, Springer, NY, pp. 529-598.

Seybert,A., R.Herrmann, and A.S.Frangakis. 2006. Structural analysis of Mycoplasma pneumoniae by cryo-electron tomography. Journal of Structural Biology *156*:342-354.

Sui,H., and K.H.Downing. 2006. Molecular architecture of axonemal microtubule doublets revealed by cryo-electron tomography. Nature *442*:475-478.

Vandenbeldt,K.J., R.M.Barnard, P.J.Hergert, X.Meng, H.Maiato, and B.F.McEwen. 2006. Kinetochores use a novel mechanism for coordinating the dynamics of individual microtubules. Curr. Biol. *16*:1217-1223.

Vidali,L., F.Chen, G.Cicchetti, Y.Ohta, and D.J.Kwiatkowski. 2006. Rac1-null mouse embryonic fibroblasts are motile and respond to platelet-derived growth factor. Mol. Biol. Cell *17*:2377-2390.

Supplementary data

Figure 3a.mov
Original tomogram of Figure 3a
Cryo-electron tomogram of actin filaments in a cell protrusion in a mouse embryonic fibroblast.

Figure 3b.mov
Original tomogram of Figure 3b
Cryo-electron tomogram of intermediate filaments, ribosomes, actin and vesicular structures in a mouse embryonic fibroblast.

Figure 3c.mov
Original tomogram of Figure 3c
Cryo-electron tomogram of microtubule plus end, actin, intermediate filaments and ribosomes in a mouse embryonic fibroblast.

Figure 3d.mov
Original tomogram of Figure 3d
Cryo-electron tomogram of mitochondria and vesicular structures in a mouse embryonic fibroblast.

Figure 4d.mov
Original tomogram of Figure 4d
Cryo-electron tomogram of frayed microtubule plus end in a mouse embryonic fibroblast.

Supplementary data are available online.